

# New insights on the massive interacting binary UU Cassiopeiae

R.E. Mennickent<sup>1</sup>, G. Djurašević<sup>2</sup>, I. Vince<sup>2</sup>, J. Garcés<sup>1</sup>, P. Hadrava<sup>3</sup>, M. Cabezas<sup>3,4</sup>, J. Petrović<sup>2</sup>, M. I. Jurković<sup>2,5</sup>, D. Korčáková<sup>6</sup>, and H. Markov<sup>7</sup>

<sup>1</sup> Universidad de Concepción, Departamento de Astronomía, Casilla 160-C, Concepción, Chile

<sup>2</sup> Astronomical Observatory Belgrade, Volgina 7, 11060 Belgrade, Serbia

<sup>3</sup> Astronomical Institute of the Academy of Sciences of the Czech Republic, Boční II 1401/1, 141 00 Praha 4, Czech Republic

<sup>4</sup> Institute of Theoretical Physics, Faculty of Mathematics and Physics, Charles University, V Holešovičkách 2, 180 00 Praha 8, Czech Republic

<sup>5</sup> Konkoly Thege Astronomical Institute, Research Center for Astronomy and Earth Sciences, Konkoly Thege Miklós út 15-17, H-1121 Budapest, Hungary

<sup>6</sup> Astronomical Institute of Charles University, V Holešovičkách 2, 180 00 Praha 8, Czech Republic

<sup>7</sup> Institute of Astronomy and NAO, Rozhen, Smolyen, Bulgaria

Received 10 April 2020 / Accepted 1 May 2020

## ABSTRACT

We present the results of the study of the close binary UU Cassiopeiae based on previously published multi wavelength photometric and spectroscopic data. Based on eclipse timings of the last 117 years, we find an improved orbital period of  $P_o = 8^d519296(8)$ . In addition, we find a long cycle of length  $T \sim 270$  d in the  $I_c$ -band data. There is no evidence for orbital period change during the last century, suggesting that the rate of mass loss from the system or mass exchange between the stars should be small. Sporadic and rapid brightness drops of up to  $\Delta V = 0.3$  mag are detected during the whole orbital cycle and infrared photometry clearly suggests the presence of circumstellar matter. We model the orbital light curve of 11 published datasets fixing the mass ratio and cool star temperature from previous spectroscopic work;  $q = 0.52$  and  $T_c = 22\,700$  K. We find a system seen at angle  $74^\circ$  with a stellar separation of  $52 R_\odot$ , a temperature for the hotter star  $T_h = 30\,200$  K and stellar masses  $17.4$  and  $9 M_\odot$ , radii  $7.0$  and  $16.9 R_\odot$  and surface gravities  $\log g = 3.98$  and  $2.94$ , for the hotter and cooler star, respectively. We find an accretion disk surrounding the more massive star, with a radius of  $21 R_\odot$  and vertical thickness in its outer edge of  $6.5 R_\odot$ , mostly occulting the hotter star. Two active regions hotter than the surrounding disk are found, one located roughly in the expected position where the stream impacts the disk and the other one in the opposite side of the disk. Changes are observed in parameters of the disk and spots in different datasets.

**Key words.** Stars: binaries: eclipsing, Stars: binaries: spectroscopic, Stars: evolution

## 1. Introduction

Massive close binaries are progenitors of many interesting objects as X-ray binaries and binary radio pulsars (Verbunt 1993), supernovae Ib and Ic (Podsiadlowski et al. 1992), as well as collapsars resulting in gamma ray bursts (Petrović et al. 2005) and gravitational wave sources (Kruckow et al. 2018). Massive binaries trace the evolutive history of these interesting objects and can explain their galactic populations (e.g. Zapartas et al. 2020). In addition, massive binaries are natural laboratories to understand the physical processes occurring during the periods of mass exchange and mass loss, that regulate their evolution determining its final fate (de Mink et al. 2014).

The eclipsing close binary UU Cassiopeiae (UU Cas, BD +60 2629, 2MASS J23503951+6054391,  $\alpha_{2000} = 23:50:39.52$ ,  $\delta_{2000} = +60:54:39.14$ ,  $V = 9.74$ , Spectral Type B0.5III)<sup>1</sup> has a distance based on the GAIA DR2 parallax of  $3256 [+392 -319]$  pc (Bailer-Jones et al. 2018). It is listed in the catalogue of massive close binaries of Polushina (2004) that compiles observable data for 176 massive close binaries with main sequence components earlier than approximately B5. In this catalogue, the object occupies the place 7th among 65 binaries with orbital period known, ordered in descending order of period length. UU Cas was studied by means of photographic spectra by Sanford (1934)

who found an orbital period  $P_o = 8^d520676$ . The General Catalog of Variable Stars<sup>2</sup> (Samus et al. 2017) gives an orbital period of  $8^d51929$  with reference to Parenago & Kukarkin (1940).

Polushina (2002) obtained *UBVR* differential magnitudes between 1984-1989 and derived stellar masses of  $34.5 \pm 1.5$  and  $25.7 \pm 0.6 M_\odot$ . She also noticed large magnitude deviations from the assumed over-contact binary model at some epochs which she has explained in terms of mass flows. In particular, she noticed the large variability of eclipse depths and overall light curve shape. The complex variability of the light curve and large deviations were ratified nine years later with new data by Kumsiashvili & Chargeishvili (2009). Using photometric observations of UU Cas obtained until year 2000, the following ephemerides is given for the primary minimum by Kreiner (2004)<sup>3</sup>:  $\text{Min I} = \text{JD } 2428751.6762 + 8^d519281 \text{ E}$ .

Gorda (2017) derived stellar masses of  $17.7$  and  $9.5 M_\odot$  assuming an orbital inclination of  $69^\circ$  and using medium resolution ( $R = 15\,000$ ) spectra. He also presented evidence for a disk surrounding the hotter component and a common expanding envelope. Recent  $H\alpha$  Doppler tomography revealed the importance of the gas flows in the semi-detached system to understand the different flux contributions. Gas stream from the cooler star, ac-

<sup>1</sup> <http://simbad.u-strasbg.fr/simbad/>

<sup>2</sup> <http://www.sai.msu.su/gcvcs/>

<sup>3</sup> <https://www.as.up.krakow.pl/o-c/index.php3>

cretion disk around the hotter star and a wind are taken into account by Kononov et al. (2019) to model the orbital variability of the  $H\alpha$  profiles. These authors and Gorda (2017) noticed that the apparent paradox of a deeper light minimum when the more massive star is occulted by the less massive star can be explained if the more massive star is surrounded by an accretion disk. The presence of a disk was already suggested by Djurašević et al. (2010) and Markov et al. (2010, 2011). The larger masses obtained by Polushina (2002) compared with those of Gorda (2017) are explained by the assumed over-contact system configuration and the absence of the disk in her model.

In this study we hope to contribute to: (1) get for the first time a physical representation of the accretion disk surrounding the more massive star and at the same time get reliable and consistent stellar and system parameters, (2) shed light on the complex photometric variability of the system and the conflicting masses obtained from previous photometric and spectroscopic studies, (3) use the photometric datasets acquired over last years by all-sky surveys and satellites to advance in the understanding of this system, (4) improve the value of the orbital period and check for its variability, and (5) get insights on the system structure using published infrared photometric data.

The paper is organized as follows: in Section 2 we give details of the photometric observations analyzed in this paper, in Section 3 we present our results based on photometric studies, in Section 4 we present the light curve model and their physical parameters, in Section 5 we discuss our findings in the context of earlier work on the system and in Section 6 we summarize our conclusions.

## 2. Observations

### 2.1. Photometric data and methodology

The photometric data used in this paper were collected from previously published articles and publicly available databases. We have studied the photometric time series found in The All-Sky Automated Survey for Supernovae ASAS-SN<sup>4</sup> in  $V$  and  $g$ , the data from Kamogata Kiso Kyoto Wide-field Survey (Machihara, H. 2014) in  $I_c$  and  $V$ . In addition, we include data acquired with The Optical Monitoring Camera (OMC, Mas-Hesse et al. 2003) on board the high-energy INTEGRAL satellite, that provides photometry in the Johnson  $V$ -band within a 5 by 5 degree field of view (Domingo et al. 2010) and it is able to detect optical sources brighter than around  $V \sim 18$ . We also include differential photometry from Kumsiashvili & Chargeishvili (2009,  $UBV$ ) and Polushina (2002,  $UBVR$ ).

We query for infrared magnitudes through the NASA/IPAC infrared science archive<sup>5</sup>. We investigated the Wide-field Infrared Survey Explorer WISE, a NASA medium class explorer mission that conducted an all-sky survey at mid-infrared band-passes centered around wavelengths 3.4, 4.6, 12 and 22  $\mu\text{m}$  (hereafter  $W1$ ,  $W2$ ,  $W3$  and  $W4$ ; Wright et al. (2010)). The survey was conducted with a 40 cm cryogenically-cooled telescope in sun-synchronous polar orbit. Four infrared detectors imaged the same sky field of view during 7.7 s ( $W1$ ,  $W2$ ) and 8.8 s ( $W3$ ,  $W4$ ). We use here the data of the second-pass processing, obtained with improved calibration and processing algorithms, superseding those obtained for the preliminary data release.

From the all aforementioned datasets we present for the first time the analysis of the INTEGRAL, ASAS-SN, KWS and

**Table 1.** Photometric time series analyzed in this paper. KW refers to Kumsiashvili & Chargeishvili (2009), KWS means Kamogata Kiso Kyoto Wide-field Survey and P02 refers to Polushina (2002). N means number of data points and  $\sigma$  average data point error.

Source	Band	$\Delta$ HJD-2400000	N	$\sigma$ (mag)
KW	$U$	42655-46055	955	NA
KW	$B$	42655-46055	955	NA
KW	$V$	42655-46055	955	NA
INTEGRAL	$V$	(1093-6774)*	3697	0.013
ASAS-SN	$V$	57009-58451	615	0.0058
ASAS-SN	$g$	58610-58795	245	0.0025
KWS	$V$	56268-58807	748	0.027
KWS	$I_c$	56484-58807	616	0.027
WISE	$W1$	(55216-55411)**	55	0.028
WISE	$W2$	(55216-55411)**	55	0.021
WISE	$W3$	(55216-55411)**	37	0.023
WISE	$W4$	(55216-55411)**	37	0.163
P02	$U$	***	47	0.028
P02	$B$	***	55	0.020
P02	$V$	***	55	0.018
P02	$R$	***	59	0.016

\* The INTEGRAL satellite data is in Barycentric Julian Date (BJD-2451544.5). \*\* The WISE satellite data is in Mean Julian Date (MJD-2400000). \*\*\* Authors give only phases versus differential magnitudes.

WISE data. Table 1 gives a summary of the data sources, the bands that were used, and the time span of the observations.

We search for periods using the GLS periodogram (Zechmeister & Kürster 2009). This algorithm uses the principle of the Lomb (1976) & Scargle (1982) periodograms with some modifications, such as the addition of a displacement in the adjustment of the fit function and the consideration of measurement errors. Compared with the classical periodogram, it gives us more accurate frequencies and a better determination of the amplitudes. We complement this analysis with the  $O - C$  method described by Sterken (2005), where predicted times of eclipses of a test ephemerides are compared with observed times in order to get an improved value of the orbital period.

Furthermore, we disentangled the light curve subtracting from the original light curve a representation of the orbital variability constructed with a Fourier series including the orbital frequency and its harmonics. This methodology was introduced in Mennickent et al. (2012) and used in several past studies of close binaries (e.g. Mennickent et al. 2019). This allowed us to search for new periodicities in the residual data. The results of this search are given in the next section.

## 3. Results

### 3.1. The orbital period

We searched for the orbital period using the  $V$ -band photometry, finding an orbital period of  $8^d519252(12)$  (Fig.1). This value compares well with that provided by Kreiner (2004), viz.  $8^d519281$ . The following ephemeris for the primary eclipse was found:

$$\text{HJD}_{\min} = 2443132.29826 + E \times 8^d519252(12) \quad (1)$$

In order to improve the accuracy of the orbital period, we selected the photometric data points with phases close to the pri-

<sup>4</sup> <http://www.astronomy.ohio-state.edu/asassn/index.shtml>

<sup>5</sup> <http://irsa.ipac.caltech.edu/Missions/wise.html>

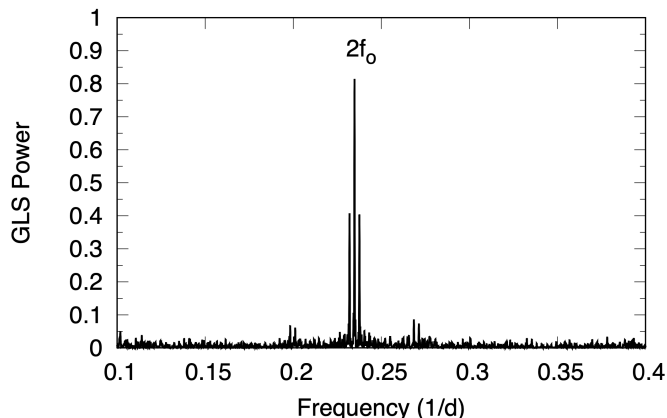


**Fig. 1.** Periodogram obtained with the V-band photometry.  $2f_0 = 2/P_0$ , where  $P_0 = 8^d519252 \pm 0^d000012$  d.

mary minimum ( $0.98 \leq \Phi_0 \leq 1.02$ ) and performed an analysis of observed (O) minus calculated (C) eclipse times following Sterken (2005). In this analysis the O-C deviations can be represented as a function of the number of cycles with a straight line whose zero point and slope are the corrections needed for the (linear) ephemeris zero point and period, respectively. We include 48 times of primary minimum studied by Kreiner (2004) and listed in the O-C Gateway<sup>6</sup>. Additionally, we include 209 new times of minima measured from the data listed in Table 1, excluding satellite data because of the different time system. The dataset of minima covers about 5000 cycles i.e. 117 years of observations. Since some minima times are published without errors, we use a simple least square fit for our analysis. Our result displayed in Fig.2 shows that the fit can be performed with a straight line, indicating a constant period. The new ephemeris is given by:

$$\text{HJD}_{\min} = 2443132.25696 + E \times 8^d519296(8) \quad (2)$$

### 3.2. Search for additional photometric periods

We disentangled the light curve removing the orbital frequency finding a long period in the residuals of the  $I_c$ -KWS band photometry;  $268.7 \pm 1.6$  d with full amplitude  $0.1096 \pm 0.0066$  mag. The following ephemeris for the minimum of the long-cycle was found:

$$\text{HJD}_{\min} = 2456493.37 + E \times (268^d7 \pm 1^d6) \quad (3)$$

No periodicity was found in the residuals of the other datasets. The periodogram showing the peak at the long cycle frequency is shown in Fig.3. The residual light curve phased with the long cycle is shown in Fig.4. The peak of the  $I_c$ -band periodogram is significant and cannot be explained in terms of the data sampling.

### 3.3. Flickering in the light curve

We observe flickering in the light curve, better represented in the INTEGRAL database (Fig.5). This phenomenon consists of drops of brightness in the light curve regarding the mean level for a given orbital phase. It was previously reported as model deviations in several bands up to 0.1 mag in earlier work with less time-resolved datasets by Polushina (2002). Larger variations of up to 0.2 mag during 9 nights between 1972 and 1973 were recorded by Kumsiashvili & Chargeishvili (2009) but interpreted in terms of an instrumental effect. The drops in brightness observed in INTEGRAL data cannot be due to measurements errors: individual data point errors are much smaller than the observed deviations and the expected instrumental error for each data point for the given system magnitude is less than 0.02 mag (Mas-Hesse et al. 2003).

A Levenberg Marquardt nonlinear curve fit was performed with two Gaussians characterized by free parameters position, full width at half maximum and area. The fit converged after 19 iterations with a  $\chi^2$  tolerance value of  $10^{-9}$  and R-square value of 0.977. The best fit reveals two different distributions separated by  $0.062 \pm 0.014$  mag and whose heights are in the ratio  $4.1 \pm 0.6$  (Fig.6). The lower distribution is  $2.4 \pm 0.3$  times broader than the tallest distribution. The areas of the distributions are  $A_1 = 11.5 \pm 1.0$  and  $A_2 = 6.8 \pm 1.5$  mag  $\times$  counts. The magnitudes in the half of the smaller distribution corresponding to larger residuals (fainter magnitudes) can be identified as fading events. The corresponding ratio of areas  $\eta = 0.5A_2/A_1$  is the relative fraction of magnitudes that can be classified as magnitude drops. We find that 29.6% of the observations corresponds to fading events in this dataset. In addition, we find that the drops occurs randomly, none periodicity was found in the residuals of INTEGRAL data. They also appear in ASAS-SN V and  $g$ -band data (Fig.7). The events have not clear dependence on the orbital phase, they appear at all phases, but seems to be more abundant in quadratures. The larger drops amount to 0.3 mag in V-band, i.e. a fall of roughly 30% of the total flux.

In order to investigate the time scale in which these fading events occur, we performed a correlation analysis measuring the temporal distance between adjacent data points and the corresponding difference of magnitude. We find that jumps in magnitude of the order of 0.1 mag already occur in time scale of minutes, and conclude that the time resolution of the data is not enough to resolve these events (Fig.8).

### 3.4. Infrared colors and W1 orbital variability

We analyzed the W1 variability and compared the infrared colors with those of Double Periodic Variables (DPVs) and Be stars. DPVs are close binaries mostly consisting of a B-type hotter star surrounded by an accretion disk fed by Roche-lobe overflow and mass transfer from a cooler giant companion Mennickent (2017). Be stars are rapidly rotating B-type stars surrounded by a circumstellar disk. Both types of objects usually show color excess mostly attributed to circumstellar reddening, therefore they are used here for comparison of presence of circumstellar matter. No correction for interstellar reddening was performed. However, at these wavelengths, the effect of interstellar reddening is negligible. In addition, we included as a reference the average colors for 136 main sequence stars in the range of spectral types from B1 V to K3 V from the Hipparcos catalogue (Perryman et al. 1997). For details of data selection of DPVs, Be stars and Hipparcos stars see Mennickent et al. (2016). Our results are shown in Fig.9.

<sup>6</sup> <http://var2.astro.cz/ocgate/index.php?lang=en>

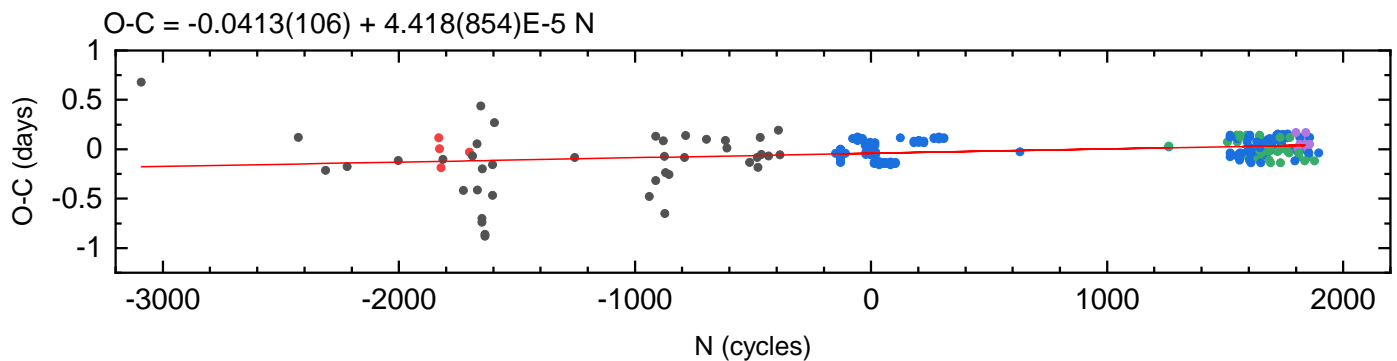


**Fig. 2.** Observed (O) minus calculated (C) epochs for primary minima versus cycle number for 117 years of observations, according to the ephemeris given by Eq. 1. Black and red dots indicate photographic and visual data, respectively. Blue, green and magenta dots show CCD or photoelectric  $V$ ,  $I_c$  and  $g$ -band data, respectively. The data points with the same X and Y coordinates are displayed with a small X offset for better visualization. See Section 3.1.

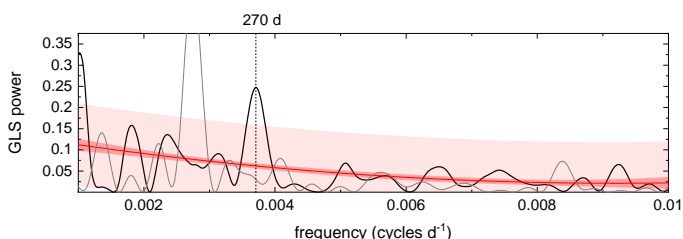


**Fig. 3.** Generalized Lomb-Scargle periodogram obtained with  $I_c$ -band data after subtraction of the orbital period. The light gray curve shows the spectral window for the data. The best 2<sup>th</sup> order polynomial fit is also shown. 95% confidence and prediction bands are shown by dashed and dashed-light areas, respectively.

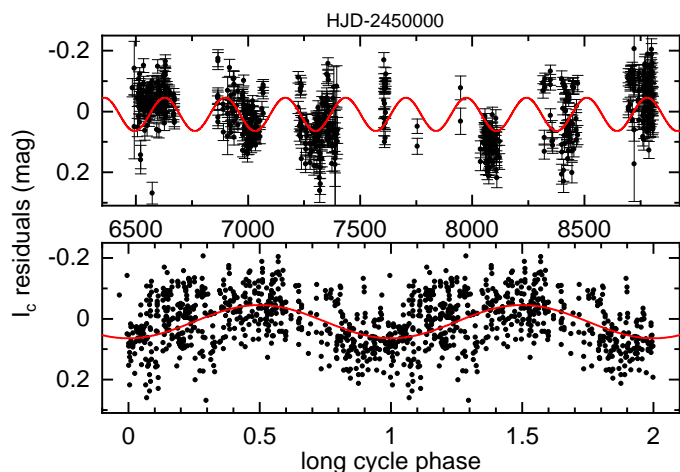


**Fig. 4.** Upper:  $I_c$ -KWS light curve after removing the orbital period. Lower: The same but phased with the long period of 269 days. The best sinus fit is also shown.

We find that the light  $W1$  magnitude follows the orbital period. Our time resolution and cadence does not allow to resolve the whole orbital cycle neither the possible long-cycle. Part of the variability occurs in longer time scales than the orbital one, this can be seen in the data acquired in the end of the time series, that deviate to brighter magnitudes compared with the rest of the data of similar orbital phase. In addition, the system appears in the  $W1 - W2$  vs.  $W2 - W3$  diagram in a place popu-

lated by systems with circumstellar envelopes, far from the place where the HIPPARCOS non-variable stars are located. This finding strongly suggests that circumstellar matter is also present in UU Cas. In addition, during the orbital cycle, the system transits mostly in the  $W1 - W2$  axis, describing a horizontal path in the color-color diagram.

The same tendency is found when comparing the published 2MASS  $J - H$  (0.194) versus  $H - K$  (0.274) colors of UU Cas (Skrutskie et al. 2006) with those of synthetic models for dwarfs and giants, along with observed colors of Be stars and DPVs (Fig.10). The UU Cas system is located in a similar place regarding the Double Periodic Variables, suggesting the existence of circumstellar matter and eventually an accretion disk.

#### 4. Light curve model

In this section we model the orbital light curves with a theoretical code that solves the inverse problem considering a semi-detached system consisting of a less massive and cooler "donor" star and a more massive and hotter "gainer" star surrounded by an accretion disk, that is both optically and geometrically thick (Djurašević 1992a,b, 1996). The model includes hot and bright spots in the disk, following evidence found in previous observations of algols (Richards 2004). These active regions influence the shape of the light curve during the ingress and egress of the eclipses. The temperature of the disk matches the gainer's one in its inner edge, and decreases with a radial profile described by an exponent  $a_T$ . The model has been described in several papers, so we remit the interested reader to Mennickent & Djurašević (2013); Mennickent et al. (2015, 2019).

We fix the donor temperature and mass ratio to  $T_c = 22\,700$  K and  $q = 0.52$ , following results from the spectroscopic studies by Kononov et al. (2019) and Gorda (2017) and also our own work based on disentangling of spectra (work in preparation). We also assume synchronous rotation for the donor, as expected for a close binary that rapidly synchronize stellar spins with the orbit due to tidal forces. On the other hand, the gainer might have been spun-up to a high rotation due to nearly tangentially infalling material (Packet 1981), hence we have assumed critical rotation for it. For  $I_c$  data, we modeled the residuals after subtracting the long cycle.

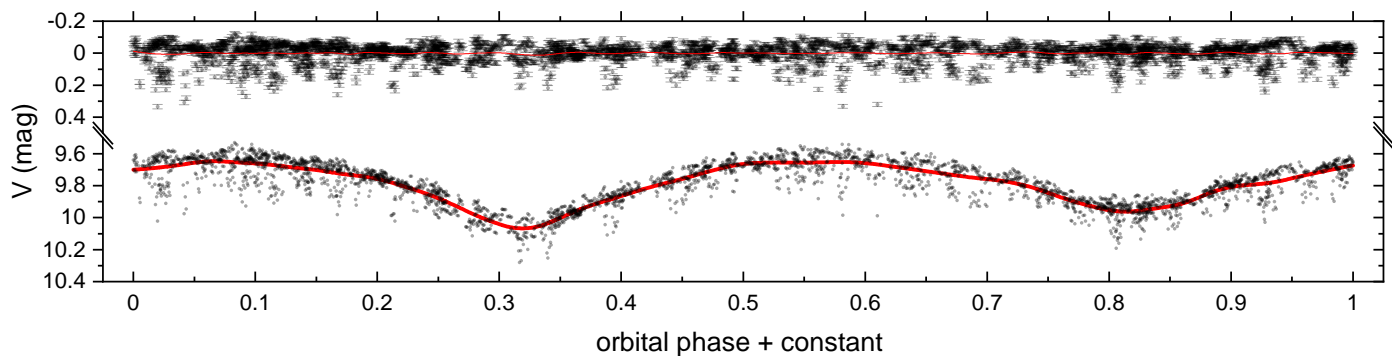


**Fig. 5.** Integral  $V$ -band data phased with the ephemeris given by Eq. 2, along with a locally weighted scatterplot smoothing curve. Residuals are shown in the upper part with data points error bars. The orbital phase has been displaced for better visualization.

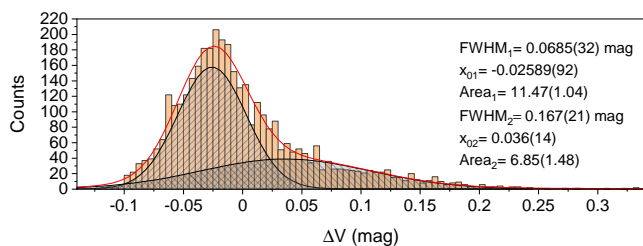


**Fig. 6.** Histogram of residuals shown in Fig. 5 modeled by the sum of two Gaussians. A non-linear fit using the Levenberg Marquardt iteration algorithm results in two distributions (black lines) and its sum (red line). The adjusted parameters full width at half maximum, center, area and their errors are given for the two Gaussians.

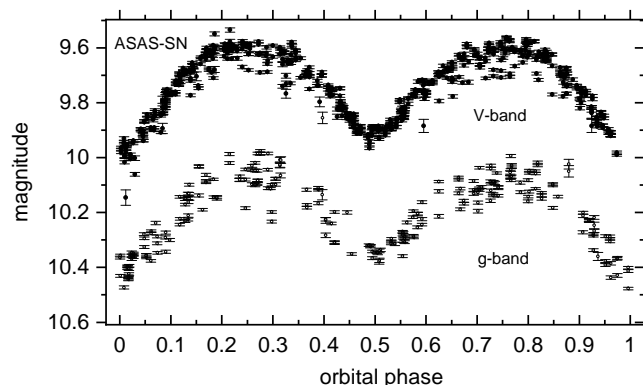


**Fig. 7.** ASAS-SN  $V$  and  $g$ -band magnitudes phased with the ephemeris given by Eq. 2. The drops in brightness seen in INTEGRAL data are also present. Phase zero corresponds to the primary (deeper) eclipse.

#### 4.1. Results of the light curve model

The parameters of the best fits are shown in Table 2.  $KWV-UBV$  and  $P02-UBVR$  multi-color data was fit independently and parameters were averaged. Examples of fits to the  $KWS-I_c$  and Integral  $V$ -band light curves are shown in Fig. 11. We obtain a good match between observed and calculated magnitudes in all studied cases, along with consistency for the stellar and orbital parameters. The disk parameters show some variations, especially the bright spot position, the spots temperature and the disk vertical thickness and radius. Our model indicates a system seen at angle  $74^\circ$  and a stellar separation of  $52 R_\odot$ . The stellar temperatures are  $22\,700\,K$  and  $30\,200\,K$ . The stellar masses are 9 and

$17.4 M_\odot$  and surface gravities  $\log g = 2.94$  and  $3.98$ . The stellar radii are  $16.9$  and  $7.0 R_\odot$ . The stellar temperatures indicate spectral types of B 2 and B 0 for the donor and gainer stars (Harmanec 1988).

The disk radius is relatively stable around a value of  $21 R_\odot$ , reaching its smaller value at  $18 R_\odot$  (INTEGRAL- $V$  data) and its maximum value at  $22 R_\odot$  (P02 data). It has a temperature of  $16\,000\,K$  at its outer edge. The inner disk thickness has an average value of  $9 R_\odot$  and the outer vertical thickness has an average value of  $6.5 R_\odot$ , being maximum at  $9.4 R_\odot$  ( $KWS-I_c$  data). The hot spot is  $36\%$  (P02 data) to  $70\%$  ( $KWS-I_c$  data) hotter than the disk and is located consistently  $42^\circ$  apart from the line joining the stellar centers in direction opposite to the orbital motion, i.e. it is located roughly at the expected region where the gas stream impacts the disk. The bright spot is  $24\%$  (P02 data) to  $50\%$  ( $KWS-I_c$  data) hotter than the disk and changes its location considerably, being located between  $82^\circ$  (KW data) and  $141^\circ$  ( $KWS-g$  data) from the line joining the stellar centers in direction of the orbital motion. At quadratures, the flux ratio between donor and disk is  $\approx 2$  in the  $I_c$ -band, while in the  $V$ -band this ratio is  $\approx 3$ . The gainer is almost completely hidden by the disk at all orbital phases contributing less than  $10\%$  to the total flux in both bands.

## 5. Discussion

Our results confirm the picture summarized by Gorda (2017) and Kononov et al. (2019) of a semidetached binary where the less massive star feeds an accretion disk located around the more massive and partly hidden star. Our light curve models based on 11 different datasets obtained at different epochs and with different photometric bands, indicate consistent results for the overall system configuration, especially the orbital and stellar parameters, consolidating the overall view of a massive interacting binary of early B-type components.

Our light curve models indicate a system of B0IV + B2III stars with a relatively large total mass of about  $26 M_\odot$ . Our stellar masses of  $17.4$  and  $9 M_\odot$  are relatively close to those reported by Gorda (2017), namely  $17.7$  and  $9.5 M_\odot$ . The mass, radius and temperature of the more massive component fit well the relationships for B-type dwarfs reported by Harmanec (1988). However, the less massive component is much larger than expected for its temperature and indicates an evolved star, consistent with its lower surface gravity. In addition, we find an accretion disk around the more massive star and derive for the first time their properties. The average disk radius of  $21 R_\odot$  means  $R_d/a \approx 0.40$ , i.e. the disk outer border is just below the tidal radius for the

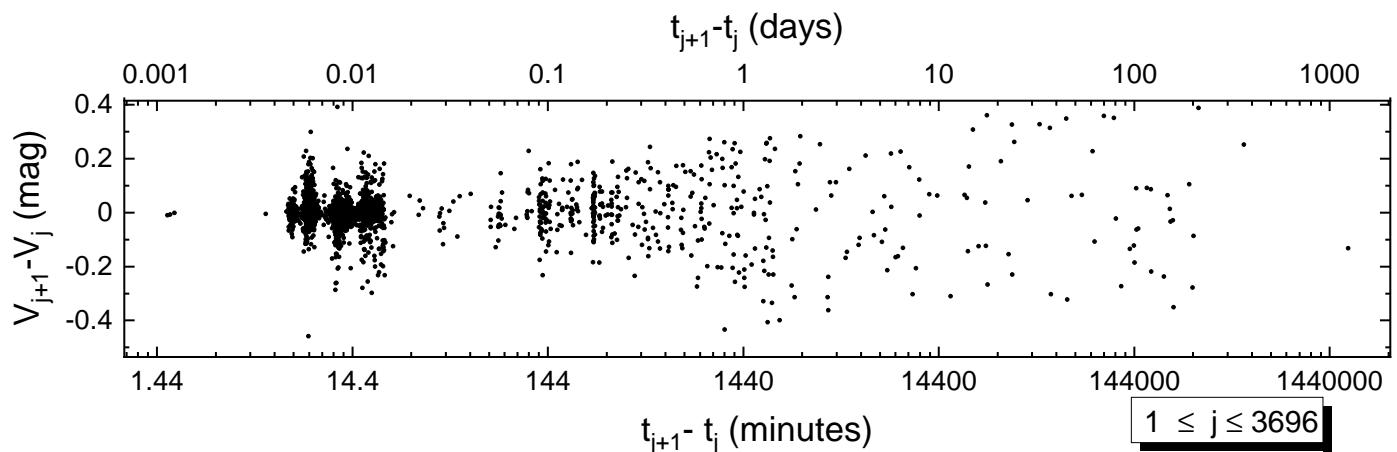


**Fig. 8.** The temporal distance between adjacent data points of all INTEGRAL V-band data is plotted against the corresponding difference of magnitude. We find that flickering occurs in time scales of minutes. Data points errors are  $\approx 0.01$  mag.

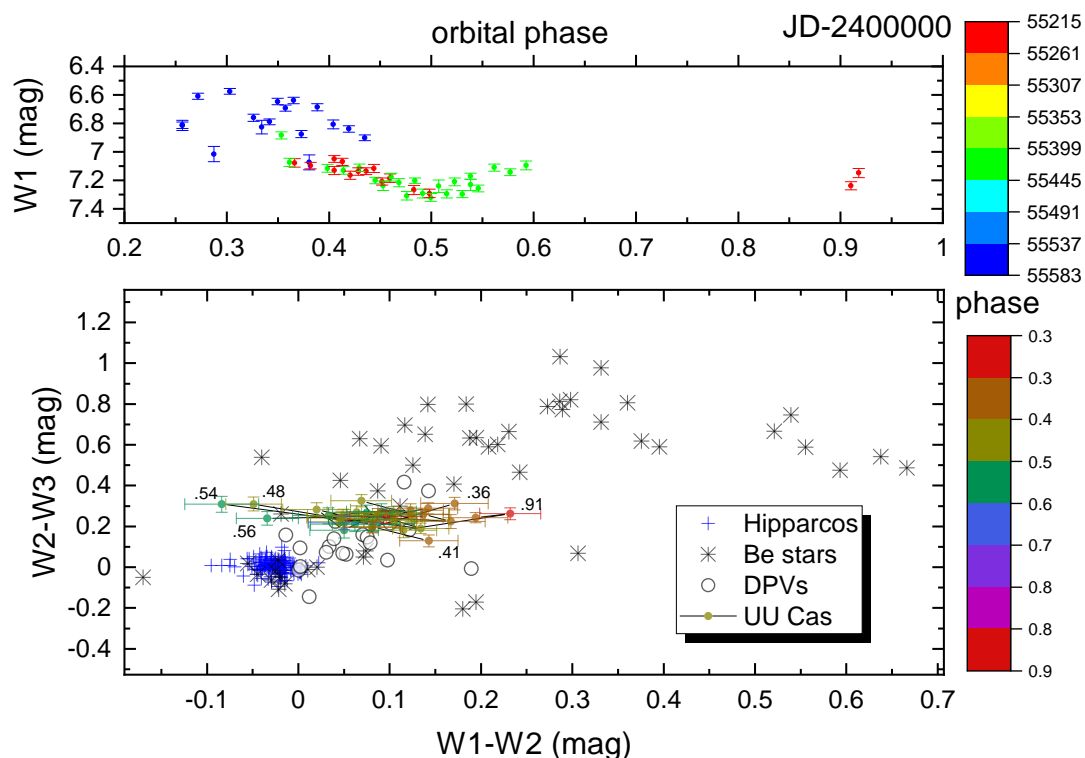


**Fig. 9.** Upper: W1 magnitude versus orbital phase according to ephemeris given by Eq. 2. Colors represent time intervals. Lower: Color-color diagram for non variable HIPPARCOS stars of spectral type B1 V - K3 V, Be stars and Double Periodic Variables (DPVs) according to Mennickent et al. (2016). The UU Cas data is added with colors along with numbers (in some cases) showing the orbital phases. Phase zero corresponds to the primary (deeper) eclipse.

given mass ratio (Paczynski 1977; Warner 1995a). The disk radius shows small changes during the observing epochs, while the disk is characterized by two hot and active photometrically variable regions. The changes in these regions (position, extension, temperature) might indicate changes in mass transfer rate modulating the mass flows and disk properties. The infrared excess obtained in our photometric study confirms the existence of circumstellar matter while the enigmatic obscuration events mostly visible in INTEGRAL V-data might be related to inhomogeneities present in the flow of mass loss. The existence of these fading events suggests a mass flow structure more complex

than provided by our simple model of disk plus two spots. In the future, new data of better accuracy could add new constraints to improve the understanding of the system.

The long period observed in the  $I_c$ -band and the light curve morphology suggest that UU Cas might be a Double Periodic Variable (DPV, Mennickent et al. 2003; Mennickent 2017), a subtype of algols showing  $\beta$ -Lyrae type light curves that have an accretion disk surrounding a B-type gainer. DPVs show long cycles of larger amplitude at red passbands (Michalska et al. 2010). This might indicate that the long cycle arises from a light source emitting mostly at redder wavelengths than the other sources in

**Table 2.** Results of the analysis of UU Cas orbital light curves. Dataset labels refers to Table 1. The models are obtained by solving the inverse problem for the Roche model with an accretion disk around the more-massive (hotter) gainer in critical non-synchronous rotation regime (Djurašević 1992a,b, 1996). Mean values are also given.

Quantity	UBV KW	UBVR P02	$g$ ASAS – SN	$V$ KWS	$I_c$ KWS	$V$ INTEGRAL	Average $\pm$ std
$q$	0.52	0.52	0.52	0.52	0.52	0.52	0.52
$i$ [°]	$74.2 \pm 0.3$	$74.7 \pm 0.3$	$74.3 \pm 0.6$	$74.3 \pm 0.4$	$74.9 \pm 0.4$	$74.6 \pm 0.5$	$74.5 \pm 0.3$
$F_d$	$0.91 \pm 0.04$	$0.97 \pm 0.03$	$0.95 \pm 0.03$	$0.88 \pm 0.02$	$0.96 \pm 0.03$	$0.80 \pm 0.03$	$0.91 \pm 0.06$
$T_d$ [K]	$16180 \pm 390$	$14970 \pm 300$	$16030 \pm 300$	$16320 \pm 300$	$16100 \pm 300$	$15720 \pm 300$	$15887 \pm 491$
$d_e$ [ $a_{\text{orb}}$ ]	$0.116 \pm 0.006$	$0.138 \pm 0.03$	$0.082 \pm 0.01$	$0.109 \pm 0.02$	$0.179 \pm 0.01$	$0.121 \pm 0.02$	$0.12 \pm 0.03$
$d_c$ [ $a_{\text{orb}}$ ]	$0.171 \pm 0.016$	$0.178 \pm 0.01$	$0.190 \pm 0.01$	$0.183 \pm 0.01$	$0.107 \pm 0.01$	$0.189 \pm 0.01$	$0.17 \pm 0.03$
$a_T$	$8.5 \pm 0.6$	$8.0 \pm 1.4$	$8.3 \pm 0.9$	$8.4 \pm 0.6$	$8.5 \pm 0.6$	$8.2 \pm 0.5$	$8.3 \pm 0.2$
$f_g$	$11.8 \pm 0.2$	$11.95 \pm 0.1$	$11.91 \pm 0.2$	$11.97 \pm 0.2$	$12.0 \pm 0.3$	$12.0 \pm 0.2$	$11.94 \pm 0.08$
$F_h$	1.00	1.00	1.00	1.00	1.00	1.00	1.00
$T_h$ [K]	$30260 \pm 400$	$30150 \pm 400$	$30260 \pm 400$	$30230 \pm 400$	$30200 \pm 400$	$30220 \pm 400$	$30220 \pm 42$
$T_c$ [K]	22700	22700	22700	22700	22700	22700	22700
$A_{\text{hs}} = T_{\text{hs}}/T_d$	$1.46 \pm 0.13$	$1.36 \pm 0.12$	$1.50 \pm 0.08$	$1.57 \pm 0.07$	$1.70 \pm 0.06$	$1.54 \pm 0.07$	$1.52 \pm 0.11$
$\theta_{\text{hs}}$ [°]	$22.8 \pm 1.2$	$24.4 \pm 0.9$	$22.9 \pm 1.2$	$22.6 \pm 1.0$	$22.8 \pm 0.9$	$23.2 \pm 1.1$	$23.1 \pm 0.7$
$\lambda_{\text{hs}}$ [°]	$313.0 \pm 5.1$	$316.5 \pm 12.8$	$326.0 \pm 7.1$	$313.5 \pm 5.6$	$320.5 \pm 6.2$	$319.1 \pm 7.1$	$318.1 \pm 4.9$
$\theta_{\text{rad}}$ [°]	$-31.0 \pm 6.1$	$-30.2 \pm 5.1$	$-27.4 \pm 5.6$	$-29.3 \pm 7.0$	$-31.8 \pm 8.2$	$-30.9 \pm 9.2$	$-30.1 \pm 1.6$
$A_{\text{bs}} = T_{\text{bs}}/T_d$	$1.31 \pm 0.05$	$1.24 \pm 0.08$	$1.40 \pm 0.08$	$1.33 \pm 0.07$	$1.50 \pm 0.08$	$1.34 \pm 0.07$	$1.35 \pm 0.09$
$\theta_{\text{bs}}$ [°]	$52.4 \pm 3.1$	$51.8 \pm 2.2$	$52.0 \pm 2.7$	$51.6 \pm 3.6$	$52.5 \pm 4.0$	$40.5 \pm 3.2$	$50.1 \pm 4.7$
$\lambda_{\text{bs}}$ [°]	$82.2 \pm 13.2$	$124.9 \pm 12.9$	$141.2 \pm 9.7$	$107.9 \pm 8.9$	$118.4 \pm 9.4$	$98.2 \pm 7.5$	$112.1 \pm 20.8$
$\Omega_h$	$9.467 \pm 0.03$	$9.554 \pm 0.02$	$9.534 \pm 0.06$	$9.562 \pm 0.05$	$9.592 \pm 0.06$	$9.586 \pm 0.05$	$9.55 \pm 0.04$
$\Omega_c$	$2.914 \pm 0.02$	$2.914 \pm 0.02$	$2.914 \pm 0.02$	$2.914 \pm 0.02$	$2.914 \pm 0.02$	$2.914 \pm 0.02$	$2.914 \pm 0.02$
$\mathcal{M}_h$ [ $M_\odot$ ]	$17.4 \pm 0.2$	$17.4 \pm 0.2$	$17.4 \pm 0.3$	$17.4 \pm 0.3$	$17.4 \pm 0.3$	$17.4 \pm 0.3$	$17.4 \pm 0.3$
$\mathcal{M}_c$ [ $M_\odot$ ]	$9.0 \pm 0.2$	$9.0 \pm 0.2$	$9.0 \pm 0.2$	$9.0 \pm 0.2$	$9.0 \pm 0.2$	$9.0 \pm 0.2$	$9.0 \pm 0.2$
$\mathcal{R}_h$ [ $R_\odot$ ]	$7.1 \pm 0.1$	$7.0 \pm 0.1$	$7.0 \pm 0.1$	$7.0 \pm 0.1$	$7.0 \pm 0.1$	$7.0 \pm 0.1$	$7.0 \pm 0.1$
$\mathcal{R}_c$ [ $R_\odot$ ]	$16.9 \pm 0.1$	$16.9 \pm 0.1$	$16.9 \pm 0.1$	$16.9 \pm 0.1$	$16.9 \pm 0.1$	$16.9 \pm 0.1$	$16.9 \pm 0.1$
$\log g_h$	$3.98 \pm 0.02$	$3.98 \pm 0.02$	$3.98 \pm 0.02$	$3.98 \pm 0.02$	$3.99 \pm 0.02$	$3.99 \pm 0.02$	$3.983 \pm 0.005$
$\log g_c$	$2.94 \pm 0.02$	$2.94 \pm 0.02$	$2.94 \pm 0.02$	$2.94 \pm 0.02$	$2.94 \pm 0.02$	$2.94 \pm 0.02$	$2.94 \pm 0.02$
$M_{\text{bol}}^h$	$-6.7 \pm 0.1$	$-6.6 \pm 0.1$	$-6.6 \pm 0.1$	$-6.6 \pm 0.1$	$-6.6 \pm 0.1$	$-6.6 \pm 0.1$	$-6.62 \pm 0.04$
$M_{\text{bol}}^c$	$-7.3 \pm 0.1$	$-7.3 \pm 0.1$	$-7.3 \pm 0.1$	$-7.3 \pm 0.1$	$-7.3 \pm 0.1$	$-7.3 \pm 0.1$	$-7.3 \pm 0.1$
$a_{\text{orb}}$ [ $R_\odot$ ]	$52.2 \pm 0.3$	$52.2 \pm 0.2$	$52.2 \pm 0.3$	$52.2 \pm 0.3$	$52.2 \pm 0.3$	$52.2 \pm 0.3$	$52.2 \pm 0.3$
$\mathcal{R}_d$ [ $R_\odot$ ]	$20.7 \pm 1.1$	$22.0 \pm 0.6$	$21.6 \pm 0.3$	$20.1 \pm 0.3$	$21.9 \pm 0.4$	$18.3 \pm 0.4$	$20.8 \pm 1.4$
$d_e$ [ $R_\odot$ ]	$6.0 \pm 0.4$	$7.2 \pm 1.2$	$4.3 \pm 0.7$	$5.7 \pm 0.5$	$9.4 \pm 0.4$	$6.3 \pm 0.4$	$6.5 \pm 1.7$
$d_c$ [ $R_\odot$ ]	$8.9 \pm 0.9$	$9.3 \pm 0.5$	$9.9 \pm 0.7$	$9.6 \pm 0.7$	$5.6 \pm 0.6$	$9.8 \pm 0.5$	$8.8 \pm 1.6$

FIXED PARAMETERS:  $q = \mathcal{M}_c/\mathcal{M}_h = 0.52$  - mass ratio of the components,  $T_c = 22\,700\text{K}$  - temperature of the less-massive (cooler) donor,  $F_c = 1.0$  - filling factor for the critical Roche lobe of the donor,  $f_c = 1.00$  - non-synchronous rotation coefficients of the donor,  $F_h = R_h/R_{zc}$  - filling factor for the critical non-synchronous lobe of the hotter, more-massive gainer (ratio of the stellar polar radius to the critical Roche lobe radius along z-axis for a star in critical non-synchronous rotation regime),  $\beta_{h,c} = 0.25$  - gravity-darkening coefficients of the components,  $A_{h,c} = 1.0$  - albedo coefficients of the components.

Note: Origin of the photometric observations, photometric band,  $q$  - mass ratio of the components,  $i$  - orbit inclination (in arc degrees),  $F_d = R_d/R_{yc}$  - disk dimension factor (the ratio of the disk radius to the critical Roche lobe radius along y-axis),  $T_d$  - disk-edge temperature,  $d_e$ ,  $d_c$  - disk thicknesses (at the edge and at the center of the disk, respectively) in the units of the distance between the components,  $a_T$  - disk temperature distribution coefficient,  $f_g$  - non-synchronous rotation coefficient of the more massive gainer (in the synchronous rotation regime),  $T_h$  - temperature of the more-massive (hotter) gainer,  $A_{h,bs} = T_{h,bs}/T_d$  - hot and bright spots' temperature coefficients,  $\theta_{h,bs}$  and  $\lambda_{h,bs}$  - spots' angular dimensions and longitudes (in arc degrees, the longitude is measured in direction of the orbital motion),  $\theta_{\text{rad}}$  - angle between the line perpendicular to the local disk edge surface and the direction of the hot-spot maximum radiation,  $\Omega_{h,c}$  - dimensionless surface potentials of the hotter gainer and cooler donor,  $\mathcal{M}_{h,c}$  [ $M_\odot$ ],  $\mathcal{R}_{h,c}$  [ $R_\odot$ ] - stellar masses and mean radii of stars in solar units,  $\log g_{h,c}$  - logarithm (base 10) of the system components effective gravity,  $M_{\text{bol}}^{h,c}$  - absolute stellar bolometric magnitudes,  $a_{\text{orb}}$  [ $R_\odot$ ],  $\mathcal{R}_d$  [ $R_\odot$ ],  $d_e$  [ $R_\odot$ ],  $d_c$  [ $R_\odot$ ] - orbital semi-major axis, disk radius and disk thicknesses at its edge and center, respectively, given in solar units.

the system. This could explain why the long cycle is detected (with small amplitude) only in the  $I_c$ -band in UU Cas. All DPVs (except  $\beta$  Lyrae) show a constant orbital period in spite of the evidence of active mass exchange and occasional mass outflows. All these credentials are similar to those of UU Cas. In addition, the ratio between the long cycle length and the orbital period is 31.7 for UU Cas, relatively close to the average  $\sim 33$  for DPVs. Since the long period is observed only in one dataset, we suggest confirmation with additional data before claiming that UU Cas is

a DPV. If confirmed, UU Cas should be the most massive DPV; typically they have total masses just around  $10 M_\odot$ .

The reported evidence for an H $\alpha$  P-Cygni like profile led Gorda (2017) to conclude that a stellar wind emerges from the system. This might indicate that the system is losing mass. However, the constancy of the orbital period through one century suggests that this mass loss should be mild, i.e. the angular momentum of the system remains almost unaltered, as well as the orbital period. This is consistent with a binary in a relatively stable and mild mass transfer stage.

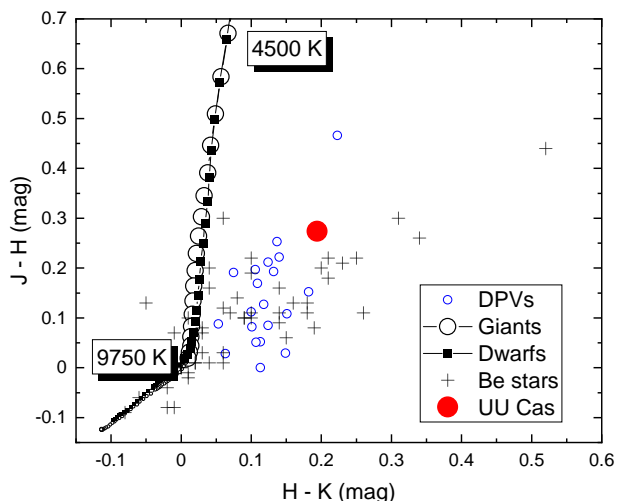


**Fig. 10.** Colors for Galactic DPVs (Mennickent et al. 2016), Be stars (Howells et al. 2001) and synthetic stellar atmosphere models with  $\log g = 4.0$  (squares with lines) and  $\log g = 3.0$  (open circles with lines) from Bessell, Castelli, & Plez (1998). The effective temperature of 2 selected synthetic models have been labeled along with the position of UU Cas.

The error in the orbital period  $\epsilon = 0^d000008$ , given by Eq. 2, might be interpreted as a possible drift of the orbital period between  $P_o - \epsilon$  and  $P_o + \epsilon$  in  $\Delta t = 117$  years. The above implies a possible change in the orbital period roughly of less than  $2\epsilon_P/\Delta t = 1.37 \times 10^{-7}$  d/yr. For conservative mass transfer this imposes an upper limit for the mass transfer rate. The expected period change in the conservative case is (Huang 1963):

$$\frac{\dot{P}_o}{P_o} = 3\dot{M}_c \left( \frac{1}{M_c} - \frac{1}{M_h} \right) \quad (4)$$

Using the aforementioned numbers and the derived stellar masses we determine  $\dot{M}_c < 1.0 \times 10^{-7} M_\odot/\text{yr}$ .

## 6. Conclusions

Based on the analysis of multi-wavelength light curves and published spectroscopic results we have arrived to the following conclusions:

- We find an improved orbital period of  $P_o = 8^d519296(8)$  that seems to be stable during the last century. This suggests that the rate of system mass loss or mass exchange between the stars should be small.
- We find a long cycle of length  $T \sim 270$  d in the  $I_c$ -band data.
- We find a system seen at angle  $74^\circ$  with a stellar separation of  $52 R_\odot$ . The stellar temperatures are  $22\,700\text{ K}$  and  $30\,200\text{ K}$ , masses  $9$  and  $17.4 M_\odot$ , radii  $16.9$  and  $7.0 R_\odot$  and surface gravities  $\log g = 2.94$  and  $3.98$ .
- The system follows a horizontal path in the  $W1 - W2$  vs.  $W2 - W3$  diagram and is located in the region of systems with circumstellar matter like DPVs and Be stars. The location in the  $J - H$  vs.  $H - K$  diagram also suggests infrared excess due to circumstellar matter.
- We find an accretion disk around the hotter star, with a radius of  $21 R_\odot$ . Two active regions are found, one located roughly in the expected position where the stream impacts the disk and the other one in the opposite side of the disk. Changes are observed in the disk and spot parameters at different datasets; this might indicate variable mass transfer rate.

- We find that the light curves show enigmatic obscuration events consisting of rapid drops of brightness of up to  $\Delta V = 0.3$  mag. These events might be related to inhomogeneities present in the flow of mass loss but more studies are needed to clarify their nature.

## Acknowledgements

We thank the anonymous referee that helped to improve the first version of this manuscript. R. E. M., J. G. and M. C. acknowledge support by BASAL Centro de Astrofísica y Tecnologías Afines (CATA) PFB-06/2007 and FONDECYT 1190621. JG acknowledges ANID project 21202285. G. D., I. V., J. P. and M. I. J. acknowledge the financial support of the Ministry of Education, Science and Technological Development of the Republic of Serbia through the contract No 451-03-68/2020/14/20002. M. C. and P. H. acknowledge support by Astronomical Institute of the Czech Academy of Sciences through the project RVO 67985815. D. K. thanks GA 17-00871S of the Czech Science Foundation. This research has made use of: (1) the SIMBAD database, operated at CDS, Strasbourg, France (Wenger et al. 2000), (2) data products from the Wide-field Infrared Survey Explorer, which is a joint project of the University of California, Los Angeles, and the Jet Propulsion Laboratory/California Institute of Technology, funded by the National Aeronautics and Space Administration, (3) the NASA/IPAC Infrared Science Archive, which is operated by the Jet Propulsion Laboratory, California Institute of Technology, under contract with the National Aeronautics and Space Administration, (4) data products from the Two Micron All Sky Survey, which is a joint project of the University of Massachusetts and the Infrared Processing and Analysis Center/California Institute of Technology, funded by the National Aeronautics and Space Administration and the National Science Foundation and (5) data from the OMC Archive at CAB (INTA-CSIC), pre-processed by ISDC.

## References

- Bailer-Jones, C. A. L., Rybizki, J., Fousneau, M., et al. 2018, *AJ*, 156, 58  
Bessell M. S., Castelli F., Plez B. 1998, *A&A*, 333, 231  
de Mink, S. E., Sana, H., Langer, N., et al. 2014, *ApJ*, 782, 7  
Djurašević G. 1992a, *Ap&SS*, 196, 267  
Djurašević G. 1992b, *Ap&SS*, 197, 17  
Djurašević G. 1996, *Ap&SS*, 240, 317  
Djurašević, G. R., Vince, I., & Atanacković, O. 2010, *Binaries - Key to Comprehension of the Universe*, 301  
Domingo, A., Gutiérrez-Sánchez, R., Rísquez, D., et al. 2010, *Astrophysics and Space Science Proceedings*, 14, 493  
Gorda, S. Y. 2017, *Astrophysical Bulletin*, 72, 321  
Harmanec P. 1988, *BAICz*, 39, 329  
Howells L., Steele I. A., Porter J. M., Etherton J. 2001, *A&A*, 369, 99  
Huang, S.-S. 1963, *ApJ*, 138, 471  
Kononov, D. A., Gorda, S. Y., & Parfenov, S. Y. 2019, *ApJ*, 883, 186  
Kreiner, J. M. 2004, *Acta Astron.*, 54, 207  
Kruckow, M. U., Tauris, T. M., Langer, N., et al. 2018, *MNRAS*, 481, 1908  
Kumsiashvili, M. I., & Chargeishvili, K. B. 2009, *arXiv e-prints*, arXiv:0907.1047  
Lomb N. R. 1976, *Ap&SS*, 39, 447 L..47M  
Markov, H., Vince, I., Markova, N., et al. 2010, *Publications de l’Observatoire Astronomique de Beograd*, 90, 159  
Markov, H., Markova, N., Vince, I., et al. 2011, *Bulgarian Astronomical Journal*, 15, 87  
Maehara, H. 2014, *JAXA research and development report*, 13, 119  
Mas-Hesse, J. M., Giménez, A., Culhane, J. L., et al. 2003, *A&A*, 411, L261  
Mennickent, R. E., Pietrzyński, G., Diaz, M., et al. 2003, *A&A*, 399, L47  
Mennickent, R. E. 2017, *Serbian Astronomical Journal*, 194, 1  
Mennickent, R. E., Kołaczowski, Z., Djurašević, G., Niemczura, E., Diaz, M., Curé, M., Araya, I., Peters, G. J. 2012, *MNRAS*, 427, 607  
Mennickent R. E., Djurašević G. 2013, *MNRAS*, 432, 799



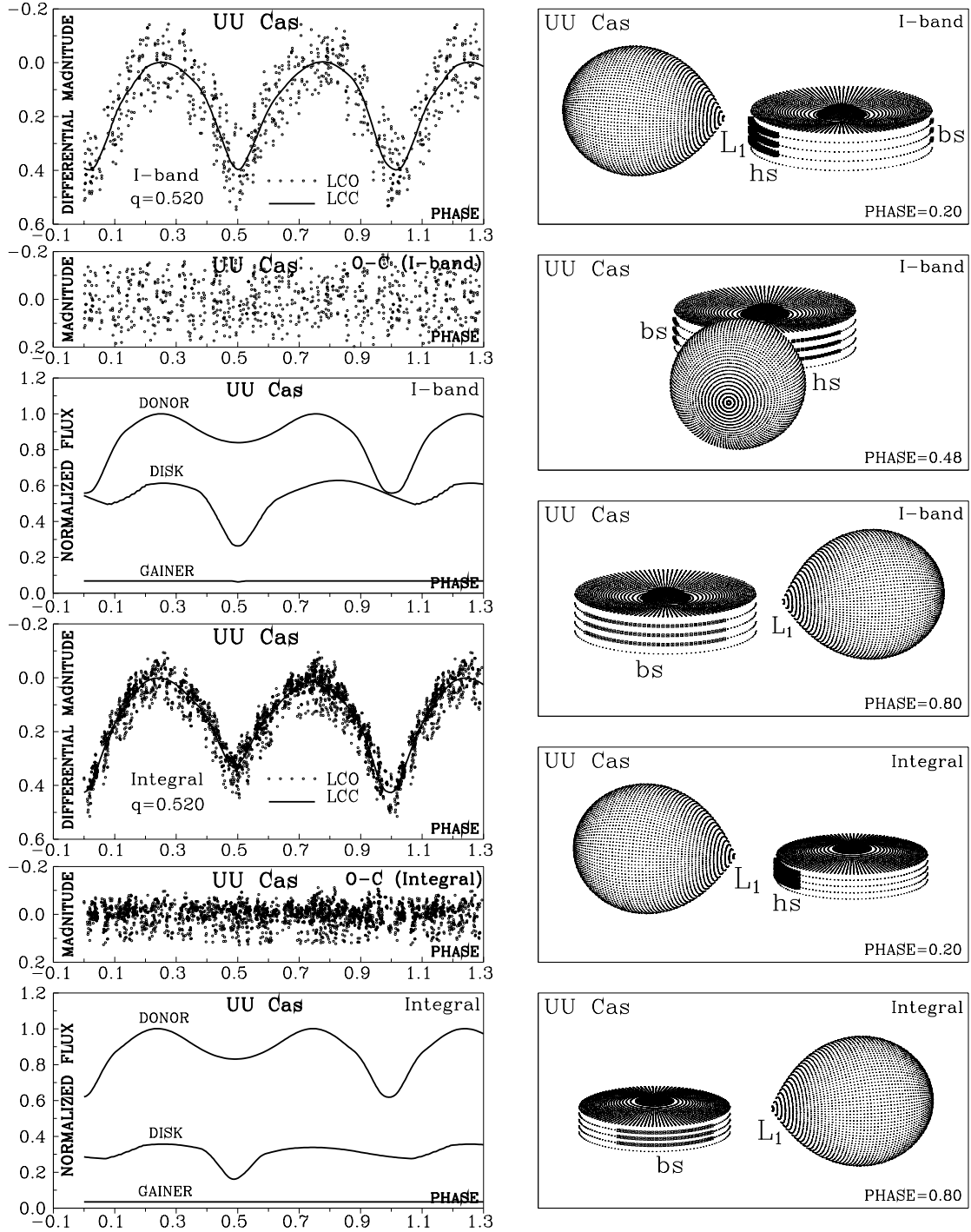


**Fig. 11.** Observed (LCO) and synthetic (LCC) light-curves of UU Cas obtained by analyzing KWS- $I_c$  data and INTEGRAL  $V$ -band photometric observations; final O-C residuals between the observed and optimum synthetic light curves; fluxes of donor, gainer and of the accretion disk, normalized to the donor flux at phase 0.25; the views of the optimal model at orbital phases 0.20, 0.48 and 0.80 ( $I_c$ -KWS) and 0.20 and 0.80 (INTEGRAL), obtained with parameters estimated by the light curve analysis.

Mennickent, R. E., Djurašević, G., Cabezas, M., Cséki, A., Rosales, J. G., Niemczura, E., Araya, I., Curé, M. 2015, MNRAS, 448, 1137  
Mennickent, R. E., Otero, S., & Kołaczkowski, Z. 2016, MNRAS, 455, 1728  
Mennickent R. E., et al. 2019, MNRAS, 487, 4169  
Michalska, G., Mennickent, R. E., Kołaczkowski, Z., et al. 2010, Binaries - Key to Comprehension of the Universe, 435, 357  
Packet, W. 1981, A&A, 102, 17  
Paczynski B. 1977, ApJ, 216, 822  
Parenago, P., Kukarkin, B. 1940, Perem Zvezdy, 5, 287  
Perryman M. A. C., et al. 1997, A&A, 323, L49

Petrovic, J., Langer, N., Yoon, S.-C., et al. 2005, A&A, 435, 247  
Podsiadlowski, P., Joss, P. C., & Hsu, J. J. L. 1992, ApJ, 391, 246  
Polushina, T. S. 2002, Astronomy Reports, 46, 900  
Polushina, T. S. 2004, Astronomical and Astrophysical Transactions, 23, 213  
Richards M. T. 2004, AN, 325, 229  
Samus, N. N., Kazarovets, E. V., Durlевич, O. V., et al. 2017, Astronomy Reports, 61, 80  
Sanford, R. F. 1934, ApJ, 79, 84  
Scargle J. D. 1982, ApJ, 263, 835  
Skrutskie M. F., et al. 2006, AJ, 131, 1163

- Sterken C. 2005, ASPC, 3, ASPC..335  
Verbunt, F. 1993, ARA&A, 31, 93  
Warner B. 1995a, Cambridge Astrophysics Series, 28  
Wenger, M., Ochsenbein, F., Egret, D., et al. 2000, A&AS, 143, 9  
Wright, E. L., Eisenhardt, P. R. M., Mainzer, A. K., et al. 2010, AJ, 140, 1868  
Zapartas, E., de Mink, S. E., Justham, S., et al. 2020, arXiv e-prints,  
arXiv:2002.07230  
Zechmeister, M., & Kürster, M. 2009, A&A, 496, 577